Fluctuations of charge separation perpendicular to the event plane and local parity violation in $\sqrt{s_{\rm NN}}$= 200 GeV Au+Au collisions at RHIC

L. Adamczyk,[1] J. K. Adkins,[23] G. Agakishiev,[21] M. M. Aggarwal,[34] Z. Ahammed,[53] I. Alekseev,[19] J. Alford,[22] C. D. Anson,[31] A. Aparin,[21] D. Arkhipkin,[4] E. Aschenauer,[4] G. S. Averichev,[21] J. Balewski,[26] A. Banerjee,[53] Z. Barnovska,[14] D. R. Beavis,[4] R. Bellwied,[49] M. J. Betancourt,[26] R. R. Betts,[10] A. Bhasin,[20] A. K. Bhati,[34] Bhattarai,[48] H. Bichsel,[55] J. Bielcik,[13] J. Bielcikova,[14] L. C. Bland,[4] I. G. Bordyuzhin,[19] W. Borowski,[45] J. Bouchet,[22] A. V. Brandin,[29] S. G. Brovko,[6] E. Bruna,[57] S. Bültmann,[32] I. Bunzarov,[21] T. P. Burton,[4] J. Butterworth,[40] H. Caines,[57] M. Calderón de la Barca Sánchez,[6] D. Cebra,[6] R. Cendejas,[35] M. C. Cervantes,[47] P. Chaloupka,[13] Z. Chang,[47] S. Chattopadhyay,[53] H. F. Chen,[42] J. H. Chen,[44] J. Y. Chen,[9] L. Chen,[9] J. Cheng,[50] M. Cherney,[12] A. Chikanian,[57] W. Christie,[4] P. Chung,[14] J. Chwastowski,[11] M. J. M. Codrington,[48] R. Corliss,[26] J. G. Cramer,[55] H. J. Crawford,[5] X. Cui,[42] S. Das,[16] A. Davila Leyva,[48] L. C. De Silva,[49] R. R. Debbe,[4] T. G. Dedovich,[21] J. Deng,[43] R. Derradi de Souza,[8] S. Dhamija,[18] B. di Ruzza,[4] L. Didenko,[4] Dilks,[35] F. Ding,[6] A. Dion,[4] P. Djawotho,[47] X. Dong,[25] J. L. Drachenberg,[52] J. E. Draper,[6] C. M. Du,[24] L. E. Dunkelberger,[7] J. C. Dunlop,[4] L. G. Efimov,[21] M. Elnimr,[56] J. Engelage,[5] K. S. Engle,[51] G. Eppley,[40] L. Eun,[25] O. Evdokimov,[10] R. Fatemi,[23] S. Fazio,[4] J. Fedorisin,[21] R. G. Fersch,[23] P. Filip,[21] E. Finch,[57] Y. Fisyak,[4] C. E. Flores,[6] C. A. Gagliardi,[47] D. R. Gangadharan,[31] D. Garand,[37] F. Geurts,[40] A. Gibson,[52] S. Gliske,[2] O. G. Grebenyuk,[25] D. Grosnick,[52] Y. Guo,[42] A. Gupta,[20] S. Gupta,[20] W. Guryn,[4] B. Haag,[6] O. Hajkova,[13] A. Hamed,[47] L-X. Han,[44] R. Haque,[53] J. W. Harris,[57] J. P. Hays-Wehle,[26] S. Heppelmann,[35] A. Hirsch,[37] G. W. Hoffmann,[48] D. J. Hofman,[10] S. Horvat,[57] B. Huang,[4] H. Z. Huang,[7] P. Huck,[9] T. J. Humanic,[31] G. Igo,[7] W. W. Jacobs,[18] C. Jena,[30] E. G. Judd,[5] S. Kabana,[45] K. Kang,[50] K. Kauder,[10] H. W. Ke,[9] D. Keane,[22] A. Kechechyan,[21] A. Kesich,[6] D. P. Kikola,[37] J. Kiryluk,[25] I. Kisel,[25] A. Kisiel,[54] D. D. Koetke,[52] T. Kollegger,[15] J. Konzer,[37] I. Koralt,[32] W. Korsch,[23] L. Kotchenda,[29] P. Kravtsov,[29] K. Krueger,[2] I. Kulakov,[25] L. Kumar,[22] R. A. Kycia,[11] M. A. C. Lamont,[4] J. M. Landgraf,[4] K. D. Landry,[7] S. LaPointe,[56] J. Lauret,[4] A. Lebedev,[4] R. Lednicky,[21] J. H. Lee,[4] W. Leight,[26] M. J. LeVine,[4] C. Li,[42] W. Li,[44] X. Li,[37] X. Li,[46] Y. Li,[50] Z. M. Li,[9] L. M. Lima,[41] M. A. Lisa,[31] F. Liu,[9] T. Ljubicic,[4] W. J. Llope,[40] R. S. Longacre,[4] X. Luo,[9] G. L. Ma,[44] Y. G. Ma,[44] D. M. M. D. Madagodagettige Don,[12] D. P. Mahapatra,[16] R. Majka,[57] S. Margetis,[22] C. Markert,[48] H. Masui,[25] H. S. Matis,[25] D. McDonald,[40] T. S. McShane,[12] S. Mioduszewski,[47] M. K. Mitrovski,[4] Y. Mohammed,[47] B. Mohanty,[30] M. M. Mondal,[47] M. G. Munhoz,[41] M. K. Mustafa,[37] M. Naglis,[25] B. K. Nandi,[17] Md. Nasim,[53] T. K. Nayak,[53] J. M. Nelson,[3] L. V. Nogach,[36] J. Novak,[28] G. Odyniec,[25] A. Ogawa,[4] K. Oh,[38] A. Ohlson,[57] V. Okorokov,[29] E. W. Oldag,[48] R. A. N. Oliveira,[41] D. Olson,[25] M. Pachr,[13] B. S. Page,[18] S. K. Pal,[53] Y. X. Pan,[7] Y. Pandit,[10] Y. Panebratsev,[21] T. Pawlak,[54] B. Pawlik,[33] H. Pei,[9] C. Perkins,[5] W. Peryt,[54] P. Pile,[4] M. Planinic,[58] J. Pluta,[54] D. Plyku,[32] N. Poljak,[58] J. Porter,[25] A. M. Poskanzer,[25] C. B. Powell,[25] C. Pruneau,[56] N. K. Pruthi,[34] M. Przybycien,[1] P. R. Pujahari,[17] J. Putschke,[56] H. Qiu,[25] S. Ramachandran,[23] R. Raniwala,[39] S. Raniwala,[39] R. L. Ray,[48] C. K. Riley,[57] H. G. Ritter,[25] J. B. Roberts,[40] O. V. Rogachevskiy,[21] J. L. Romero,[6] J. F. Ross,[12] A. Roy,[53] L. Ruan,[4] J. Rusnak,[14] N. R. Sahoo,[53] P. K. Sahu,[16] I. Sakrejda,[25] S. Salur,[25] A. Sandacz,[54] J. Sandweiss,[57] E. Sangaline,[6] A. Sarkar,[17] J. Schambach,[48] R. P. Scharenberg,[37] A. M. Schmah,[25] B. Schmidke,[4] N. Schmitz,[27] T. R. Schuster,[15] J. Seger,[12] P. Seyboth,[27] N. Shah,[7] E. Shahaliev,[21] M. Shao,[42] B. Sharma,[34] M. Sharma,[56] W. Q. Shen,[44] S. S. Shi,[9] Q. Y. Shou,[44] E. P. Sichtermann,[25] R. N. Singaraju,[53] M. J. Skoby,[18] D. Smirnov,[4] N. Smirnov,[57] D. Solanki,[39] P. Sorensen,[4] U. G. deSouza,[41] H. M. Spinka,[2] B. Srivastava,[37] T. D. S. Stanislaus,[52] J. R. Stevens,[26] R. Stock,[15] M. Strikhanov,[29] B. Stringfellow,[37] A. A. P. Suaide,[41] M. C. Suarez,[10] M. Sumbera,[14] X. M. Sun,[25] Y. Sun,[42] Z. Sun,[24] B. Surrow,[46] D. N. Svirida,[19] T. J. M. Symons,[25] A. Szanto de Toledo,[41] J. Takahashi,[8] A. H. Tang,[4] Z. Tang,[42] L. H. Tarini,[56] T. Tarnowsky,[28] J. H. Thomas,[25] A. R. Timmins,[49] D. Tlusty,[14] M. Tokarev,[21] S. Trentalange,[7] R. E. Tribble,[47] P. Tribedy,[53] B. A. Trzeciak,[54] O. D. Tsai,[7] J. Turnau,[33] T. Ullrich,[4] D. G. Underwood,[2] G. Van Buren,[4] G. van Nieuwenhuizen,[26] J. A. Vanfossen, Jr.,[22] R. Varma,[17] G. M. S. Vasconcelos,[8] R. Vertesi,[14] F. Videbæk,[4] Y. P. Viyogi,[53] S. Vokal,[21] S. A. Voloshin,[56] A. Vossen,[18] M. Wada,[48] M. Walker,[26] F. Wang,[37] G. Wang,[7] H. Wang,[4] J. S. Wang,[24] Q. Wang,[37] X. L. Wang,[42] Y. Wang,[50] G. Webb,[23] J. C. Webb,[4] G. D. Westfall,[28] H. Wieman,[25] S. W. Wissink,[18] R. Witt,[51] Y. F. Wu,[9] Z. Xiao,[50] W. Xie,[37] K. Xin,[40] H. Xu,[24] N. Xu,[25] Q. H. Xu,[43] W. Xu,[7] Y. Xu,[42] Z. Xu,[4] Yan,[50] C. Yang,[42] Y. Yang,[24] Y. Yang,[9] P. Yepes,[40] L. Yi,[37] K. Yip,[4] I-K. Yoo,[38] Y. Zawisza,[42] H. Zbroszczyk,[54] W. Zha,[42] J. B. Zhang,[9] S. Zhang,[44] X. P. Zhang,[50] Y. Zhang,[42] Z. P. Zhang,[42] F. Zhao,[7] J. Zhao,[44] C. Zhong,[44] X. Zhu,[50] Y. H. Zhu,[44] Y. Zoulkarneeva,[21] and M. Zyzak[25]

(STAR Collaboration)

[1]AGH University of Science and Technology, Cracow, Poland
[2]Argonne National Laboratory, Argonne, Illinois 60439, USA
[3]University of Birmingham, Birmingham, United Kingdom
[4]Brookhaven National Laboratory, Upton, New York 11973, USA
[5]University of California, Berkeley, California 94720, USA
[6]University of California, Davis, California 95616, USA
[7]University of California, Los Angeles, California 90095, USA
[8]Universidade Estadual de Campinas, Sao Paulo, Brazil
[9]Central China Normal University (HZNU), Wuhan 430079, China
[10]University of Illinois at Chicago, Chicago, Illinois 60607, USA
[11]Cracow University of Technology, Cracow, Poland
[12]Creighton University, Omaha, Nebraska 68178, USA
[13]Czech Technical University in Prague, FNSPE, Prague, 115 19, Czech Republic
[14]Nuclear Physics Institute AS CR, 250 68 Řež/Prague, Czech Republic
[15]University of Frankfurt, Frankfurt, Germany
[16]Institute of Physics, Bhubaneswar 751005, India
[17]Indian Institute of Technology, Mumbai, India
[18]Indiana University, Bloomington, Indiana 47408, USA
[19]Alikhanov Institute for Theoretical and Experimental Physics, Moscow, Russia
[20]University of Jammu, Jammu 180001, India
[21]Joint Institute for Nuclear Research, Dubna, 141 980, Russia
[22]Kent State University, Kent, Ohio 44242, USA
[23]University of Kentucky, Lexington, Kentucky, 40506-0055, USA
[24]Institute of Modern Physics, Lanzhou, China
[25]Lawrence Berkeley National Laboratory, Berkeley, California 94720, USA
[26]Massachusetts Institute of Technology, Cambridge, MA 02139-4307, USA
[27]Max-Planck-Institut für Physik, Munich, Germany
[28]Michigan State University, East Lansing, Michigan 48824, USA
[29]Moscow Engineering Physics Institute, Moscow Russia
[30]National Institute of Science Education and Research, Bhubaneswar 751005, India
[31]Ohio State University, Columbus, Ohio 43210, USA
[32]Old Dominion University, Norfolk, VA, 23529, USA
[33]Institute of Nuclear Physics PAN, Cracow, Poland
[34]Panjab University, Chandigarh 160014, India
[35]Pennsylvania State University, University Park, Pennsylvania 16802, USA
[36]Institute of High Energy Physics, Protvino, Russia
[37]Purdue University, West Lafayette, Indiana 47907, USA
[38]Pusan National University, Pusan, Republic of Korea
[39]University of Rajasthan, Jaipur 302004, India
[40]Rice University, Houston, Texas 77251, USA
[41]Universidade de Sao Paulo, Sao Paulo, Brazil
[42]University of Science & Technology of China, Hefei 230026, China
[43]Shandong University, Jinan, Shandong 250100, China
[44]Shanghai Institute of Applied Physics, Shanghai 201800, China
[45]SUBATECH, Nantes, France
[46]Temple University, Philadelphia, Pennsylvania, 19122, USA
[47]Texas A&M University, College Station, Texas 77843, USA
[48]University of Texas, Austin, Texas 78712, USA
[49]University of Houston, Houston, TX, 77204, USA
[50]Tsinghua University, Beijing 100084, China
[51]United States Naval Academy, Annapolis, MD 21402, USA
[52]Valparaiso University, Valparaiso, Indiana 46383, USA
[53]Variable Energy Cyclotron Centre, Kolkata 700064, India
[54]Warsaw University of Technology, Warsaw, Poland
[55]University of Washington, Seattle, Washington 98195, USA
[56]Wayne State University, Detroit, Michigan 48201, USA
[57]Yale University, New Haven, Connecticut 06520, USA
[58]University of Zagreb, Zagreb, HR-10002, Croatia

Previous experimental results based on data ($\sim$ 15 million events) collected by the STAR detector at RHIC suggest event-by-event charge separation fluctuations perpendicular to the event plane in non-central heavy-ion collisions. Here we present the correlator previously used split into its two component parts to reveal correlations parallel and perpendicular to the event plane. The results are from a high statistics 200 GeV Au+Au collisions data set (57 million events) collected by

the STAR experiment. We explicitly count units of charge separation from which we find clear evidence for more charge separation fluctuations perpendicular than parallel to the event plane. We also employ a modified correlator to study the possible $\mathcal{P}$-even background in same and opposite charge correlations, and find that the $\mathcal{P}$-even background may largely be explained by momentum conservation and collective motion.

PACS numbers: 11.30.Er, 11.30.Qc, 25.75.Ld, 25.75.Nq

I. INTRODUCTION

Parity violation represents a preference of handedness in nature. It may be violated globally or locally. In the global sense, the weak interactions of the standard model are parity odd [1] while the strong interactions are parity even at vanishing temperature and isospin density [2]. However, it has been found possible for parity to be violated locally in microscopic domains in QCD at finite temperature [3, 4]. Parity-odd ($\mathcal{P}$-odd) domains in QCD are the consequence of topologically non-trivial configurations of gauge fields. A particular domain may be characterized by its topological charge. States with positive and negative topological charge both violate parity but with an opposite observable pattern. Only states with zero topological charge conserve parity. The global conservation of parity in QCD occurs since positive and negative topological charge states are equally probable in nature.

The hot, dense, and deconfined QCD matter produced at RHIC is a natural place to study such $\mathcal{P}$-odd domains. A hypothesis has been made stating that these $\mathcal{P}$-odd domains might be observable in heavy-ion collisions. The so called *Chiral Magnetic Effect* (CME) states that $\mathcal{P}$-odd domains can interact with the very large magnetic fields in non-central collisions yielding charge-separation parallel to the system's orbital angular momentum [5–8]. This can be viewed as the creation of an electric dipole moment vector perpendicular to the reaction plane (the plane which contains the impact parameter and the beam momenta). In practice, the estimated reaction plane is called the event plane.

For a given sign of topological charge and magnetic field, the sign of the electric dipole moment produced by the CME is also fixed (parity violation). However, positive and negative topological charges are equally likely and cannot be distinguished on an event-by-event basis. One therefore expects the CME to instead manifest itself in an experiment as charge-separation *fluctuations* perpendicular to the reaction plane.

Previous STAR results based on 15 million Au+Au events at 200 GeV from RHIC 2004 data reported an experimental observation of the charge-separation fluctuations possibly providing an evidence for the CME [9, 10]. A comparable signal was observed by the ALICE experiment with 13 million Pb+Pb events at 2.76 TeV [11]. Besides higher statistics analyzed, this article complements the previous publications in two principle ways. First, we present the correlator, $\langle\cos(\phi_\alpha + \phi_\beta - 2\Psi_{\rm RP})\rangle$, split into its in-plane and out-of-plane components (See Eq. 1). Second, we compare the correlator previously used to a modified correlator. The comparison enables a better understanding of the suppression of opposite w.r.t. same charge correlations measured with $\langle\cos(\phi_\alpha + \phi_\beta - 2\Psi_{\rm RP})\rangle$.

This article is divided into six sections. In Sec. II we describe the STAR experimental setup and data taking conditions used in this analysis. In Sec. III we describe the methodology of the analysis including the definitions of correlations measured. In Sec. IV we discuss the systematic uncertainties which mainly arise due to event plane resolution uncertainties in the modified correlator. In Sec. V we present our results. Finally in Sec. VI we summarize our results.

II. EXPERIMENTAL SETUP AND DATA TAKING

In this analysis, 57 million minimum bias events taken by the STAR detector [12] at RHIC during the 2007 Au+Au run at $\sqrt{s_{\rm NN}}$= 200 GeV are used. A hadronic minimum bias trigger was formed by requiring a spectator neutron signal above the threshold value in both zero-degree calorimeters (ZDC). Two ZDC shower maximum detectors (ZDC-SMD) measure the spectator neutron spatial distributions. The ZDC-SMDs are located in the beam rapidity regions [13]. Charged particles were tracked primarily with the STAR Time Projection Chamber (TPC). Tracks are retained if their transverse momentum and pseudorapidity are in the range $0.15 < p_T < 2$ GeV/c and $|\eta| < 1.0$, respectively. Event and track cuts are chosen to be the same as in the previous STAR publications on this subject [9, 10]. Centrality in this data set is determined from the global tracking of charged particles satisfying specific track quality cuts in the pseudorapidity region $|\eta| < 0.5$ and with the distance of closest approach (DCA) to the primary-vertex less than 3 cm [14].

III. METHOD OF ANALYSIS

The correlation function used in our previous publication to search for the CME is given by [15]:

$$\begin{aligned} & \langle\cos(\phi_\alpha + \phi_\beta - 2\Psi_{\rm RP})\rangle \\ = \; & \langle\cos(\Delta\phi_\alpha)\cos(\Delta\phi_\beta) - \sin(\Delta\phi_\alpha)\sin(\Delta\phi_\beta)\rangle \\ = \; & [\langle v_{1,\alpha} v_{1,\beta}\rangle + B_{\rm IN}] - [\langle a_{1,\alpha} a_{1,\beta}\rangle + B_{\rm OUT}]. \end{aligned} \quad (1)$$

The averaging is done over all particles in an event and over all events. ϕ_α and ϕ_β are the azimuthal angles of particles α and β, respectively. $\Psi_{\rm RP}$ represents the azimuthal angle of the reaction plane and $\Delta\phi = (\phi - \Psi_{\rm RP})$. $B_{\rm IN}$ and $B_{\rm OUT}$ represent $\mathcal{P}$-even background processes which may or may not cancel. v_1 and a_1 are the first harmonic coefficients in the Fourier decomposition of the azimuthal distribution of particles of a given transverse momentum and rapidity:

$$\begin{aligned}\frac{dN_\alpha}{d\phi} \;\propto\; & 1 + 2v_{1,\alpha}\cos(\Delta\phi) + 2v_{2,\alpha}\cos(2\Delta\phi) + ... \\ & + \; 2a_{1,\alpha}\sin(\Delta\phi) + 2a_{2,\alpha}\sin(2\Delta\phi) + ... \end{aligned} \quad (2)$$

Conventionally we call v_1 "directed flow" and v_2 "elliptic flow".

We refer to Eq. 1 as the *three-point correlator*. Since the reaction plane is not directly measurable we estimate it using event planes. The event planes are calculated from the particle distributions themselves,

$$\Psi_n = \frac{1}{n}\tan^{-1}\left[\frac{\sum w_i \sin(n\phi_i)}{\sum w_i \cos(n\phi_i)}\right], \quad (3)$$

where n is the harmonic and w_i is a weight for each particle i in the sum [16]. The weight is chosen to be the p_T of the particle itself when $0.15 < p_T < 2$ GeV/c to increase the event plane resolution. Above 2 GeV/c, the weight is set to 2. A first harmonic event plane (Ψ_1) is obtained from the spectator neutron distributions detected in the STAR ZDC-SMD [13]. This type of event plane exploits the directed flow of spectator neutrons measured at very forward rapidity. A second harmonic event plane (Ψ_2) is obtained by exploiting the large elliptic flow of charged hadrons measured at mid-rapidity in the TPC, and is also called "the participant plane". The difference between Ψ_1 and Ψ_2 mainly lies in the event-by-event fluctuations [17], and presents a major systematic uncertainty in this paper.

As the CME causes charge separation fluctuations perpendicular to the reaction plane, it is the sine part of the three-point correlator which is sensitive to the CME. Note that the cosine part serves to establish a reference or baseline to the measurement since both parts are equally sensitive to backgrounds unrelated to the reaction plane. In this article we present measurements of both parts.

The three-point correlator weights different azimuthal regions of charge separation differently, i.e. oppositely charged pairs which are emitted azimuthally at 90° from the event plane (maximally out-of-plane) are weighted more heavily than those emitted only a few degrees from the event plane (minimally out-of-plane). We wish to modify the three-point correlator such that all azimuthal regions of charge separation are weighted identically. The modification, in particular, allows us to better understand the source of the suppression of opposite charge correlations seen previously [9, 10].

This may be done by first rewriting Eq. 1 as

$$\langle\cos(\phi_\alpha + \phi_\beta - 2\Psi_{\rm RP})\rangle = \langle(M_\alpha M_\beta S_\alpha S_\beta)_{\rm IN}\rangle - \langle(M_\alpha M_\beta S_\alpha S_\beta)_{\rm OUT}\rangle\,, \quad (4)$$

where M and S stand for the absolute magnitude ($0 \leq M \leq 1$) and sign (±1) of the sine or cosine function, respectively. IN represents the cosine part of Eq. 1 (in-plane) and OUT represents the sine part of Eq. 1 (out-of-plane).

To study the dependence of expression 4 on M we compare the correlations obtained to those of a reduced version:

$$\left(\frac{\pi}{4}\right)^2\left(\langle S_\alpha S_\beta\rangle_{\rm IN} - \langle S_\alpha S_\beta\rangle_{\rm OUT}\right) \equiv \text{msc}. \quad (5)$$

We refer to Eq. 5 as a modulated sign correlation (msc). The transition from Eq. 4 to Eq. 5 can be seen with the following two reductions: $\langle MS\rangle \to \langle M\rangle\langle S\rangle$ and $\langle M_\alpha M_\beta\rangle \to \langle M\rangle^2$. $\langle S_\alpha S_\beta\rangle$ may be written as sum of terms involving Fourier coefficients of which only the odd harmonics contribute. The common coefficient for all contributions is $(4/\pi)^2$ with a pre-factor of $1/n$, where n is the order of the harmonic. For this reason we choose $\langle M_{\rm IN}\rangle^2 = \langle M_{\rm OUT}\rangle^2 = (\pi/4)^2$. With this choice, the msc is also given by the far right hand side of Eq. 1 when the $n = 1$ Fourier coefficients dominate over the other odd coefficients. The msc differs from the three-point correlator in the inclusion of higher harmonics and in the removal of "magnitude correlations" (correlations of M_α with M_β), which are of "non-flow" origin. By non-flow, we mean the correlations not related to the orientation of the reaction plane. Since the msc is not a pure harmonic, its event plane resolution correction is also not generally localized within one harmonic. However, we are justified in using the same correction so long as $a_1 \gg a_n/n$ and $v_1 \gg v_n/n$ ($n = 3, 5, 7...$) or if at least a_n fluctuations are similar in magnitude as v_n fluctuations. We correct both the three-point correlator as well as the msc with a second harmonic sub-event plane resolution, $\langle\cos(2(\Psi_a - \Psi_b))\rangle^{1/2}$, where Ψ_a and Ψ_b are the event plane angles in sub-event a and b, respectively. We discuss the systematic uncertainties associated with this correction applied to the msc in Sec. IV.

For a known reaction plane, $\langle S_\alpha S_\beta\rangle$ is given simply by the net number of particle pairing combinations divided by the total number of combinations. The net number of particle pairing combinations is defined as the difference in the number of same side and opposite side combinations. For the same charge in-plane correlations we have

$$\langle S_\alpha S_\beta\rangle_{\rm IN} = \frac{N_\delta^{\rm L}\left(N_\delta^{\rm L}-1\right) + N_\delta^{\rm R}\left(N_\delta^{\rm R}-1\right) - 2N_\delta^{\rm L}N_\delta^{\rm R}}{N_\delta\left(N_\delta - 1\right)}, \quad (6)$$

where $\delta = +$ for $\alpha\beta = ++$, and $\delta = -$ for $\alpha\beta = --$. For opposite charge in-plane correlations we have

$$\langle S_\alpha S_\beta\rangle_{\rm IN} = \frac{N_+^{\rm L}N_-^{\rm L} + N_+^{\rm R}N_-^{\rm R} - N_+^{\rm L}N_-^{\rm R} - N_-^{\rm L}N_+^{\rm R}}{N_+N_-}. \quad (7)$$

Here N stands for the number of particles detected either on the left (L) or right (R) of the perpendicular to the

reaction plane in the transverse plane and with a positive (+) or negative (-) charge. For out-of-plane correlations one simply replaces L and R with T and B (top and bottom of the reaction plane in the transverse plane).

To avoid self correlations where a particle is trivially correlated with an event plane calculated in the same particle pool, we use two equal multiplicity sub-events to calculate the msc. The sub-events are statistically independent with random particle assignments. With sub-events, the azimuthal locations (T, B, L, R) of the particles from one sub-event are calculated with respect to the sub-event plane from the other sub-event.

A. Charge separation counting

Units of in-plane and out-of-plane charge separation are defined as

$$\begin{aligned} \Delta Q_{\rm IN} &= \left(N_+^{\rm L} - N_-^{\rm L}\right) - \left(N_+^{\rm R} - N_-^{\rm R}\right), \\ \Delta Q_{\rm OUT} &= \left(N_+^{\rm T} - N_-^{\rm T}\right) - \left(N_+^{\rm B} - N_-^{\rm B}\right), \end{aligned} \tag{8}$$

respectively. They can be understood as the net charge on one side of the event plane minus the net charge on the opposite side of the event plane. The choice of sign for ΔQ is irrelevant here.

Equation 5 like Eq. 1 is sensitive to $\mathcal{P}$-even correlations not related to charge separation. With the aim of separating out the simplest effects of charge separation fluctuations from other $\mathcal{P}$-even backgrounds we express the msc in terms of states of observed charge separation ΔQ. By simplest we mean the contribution to Eq. 5 which arises from different $\Delta Q_{\rm OUT}$ and $\Delta Q_{\rm IN}$ probability distributions. We rearrange the msc into two terms:

$$\mathrm{msc} = \Delta\mathrm{msc} + \Delta N \tag{9}$$

$$\Delta\mathrm{msc} = \frac{1}{N_{\rm E}} \sum_{\Delta Q} \langle N(\Delta Q)\rangle \left[\mathrm{msc}_{\rm IN}(\Delta Q) - \mathrm{msc}_{\rm OUT}(\Delta Q)\right] \tag{10}$$

$$\Delta N = \frac{1}{N_{\rm E}} \sum_{\Delta Q} \langle \mathrm{msc}(\Delta Q)\rangle \left[N_{\rm IN}(\Delta Q) - N_{\rm OUT}(\Delta Q)\right], \tag{11}$$

where the sum goes over all observed units of charge-separation. $N_{\rm E}$ stands for the total number of events. $N_{\rm IN}(\Delta Q)$ stands for the number of events with ΔQ units of in-plane charge separation, and $\mathrm{msc}_{\rm IN}(\Delta Q)$ stands for the $\langle\mathrm{msc}\rangle$ in those events. The averages, $\langle N(\Delta Q)\rangle = (N_{\rm IN}(\Delta Q) + N_{\rm OUT}(\Delta Q))/2$ and $\langle \mathrm{msc}(\Delta Q)\rangle = (\mathrm{msc}_{\rm IN}(\Delta Q) + \mathrm{msc}_{\rm OUT}(\Delta Q))/2$, represent an average over in-plane and out-of-plane parts.

A given ΔQ state will be a superposition of many different configurations or sub-states. The sub-states may be described in terms of an underlying neutral pairing of particles plus the residual net charge on each side (T, B, L or R). The underlying neutral pairs are formed by pairing up positively and negatively charged particles on a particular side until only a residual net charge remains. The residual net charge in a given ΔQ bin may also be arranged in several ways. For example, consider the state

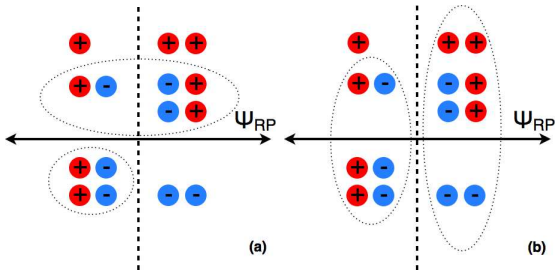

FIG. 1: (Color online) Example of a charge configuration with the underlying neutral pairing enclosed by dotted ovals. (a) shows the procedure for counting $\Delta Q_{\rm OUT} = +5$. (b) shows the same event but with the procedure for counting $\Delta Q_{\rm IN} = +1$.

$\Delta Q_{\rm IN} = +2$. The residual net charge is +2 units. One sub-state is the case when the left side has a net charge of +2 and the right side has a net charge of 0 (neutral). Another sub-state is formed with a net charge of -2 on the right and 0 on the left. The other sub-state occurs when the left side has +1 and the right side has -1 units of net charge. The idea of charge separation counting is illustrated in Fig. 1. Both the underlying neutral pairing and the residual net charge contribute to the overall configuration within each ΔQ bin.

The right hand side of Eq. 9 is composed of two terms. The first term, Δmsc, is sensitive to the difference between in-plane and out-of-plane ΔQ configurations $(\mathrm{msc}_{\rm IN}(\Delta Q) - \mathrm{msc}_{\rm OUT}(\Delta Q))$. The second term, ΔN, is sensitive to the difference between in-plane and out-of-plane ΔQ probabilities $(N_{\rm IN}(\Delta Q) - N_{\rm OUT}(\Delta Q))$. The factor, $N_{\rm IN}(\Delta Q) - N_{\rm OUT}(\Delta Q)$, is of course identical for same and opposite charge correlations. Therefore, the difference between same and opposite charge ΔN correlations is determined exclusively by the prefactor $\langle\mathrm{msc}(\Delta Q)\rangle$. If the CME does not significantly alter the charge-separation sub-states it will be isolated in the ΔN term of Eq. 9. In general, both terms could be affected by a $\mathcal{P}$-even background and neither is to be regarded as an isolation of a $\mathcal{P}$-even background.

The effects of $\mathcal{P}$-even local charge conservation and momentum conservation coupled with non-zero v_2 has been shown to yield a substantial background to the same and opposite charge correlations of Eq. 1 [18, 19]. The contribution of this effect to Eq. 5 should be reduced due to the treatment of the magnitudes of the cosine and sine functions.

B. Acceptance effects

Anisotropic or imperfect detector acceptance may also induce false correlations. The STAR detector has nearly complete azimuthal coverage but nevertheless we apply a re-centering correction [20] to all the event plane calculations. The correction is done in bins of centrality, location of collision parallel to the beam axis, and STAR run

number which represents a period of time with constant detector calibrations. Particles α and β in the three-point correlator are also re-centered. The effect of this procedure was only found to be sizable in the most central bins where the signal is small.

IV. SYSTEMATIC UNCERTAINTIES

We estimate the systematic uncertainties on our measurements by comparing results obtained using TPC and ZDC-SMD event planes. The difference between these two measurements forms our estimate of the systematic uncertainty. This estimate is shown in the shaded bands in Figs. 5 and 7. For the three-point correlator, these values characterize non-flow uncertainties in the reaction plane reconstruction. For the ΔN and Δmsc terms the values characterize both non-flow uncertainties in the reaction plane reconstruction as well as uncertainties in applying the 2^{nd} harmonic event plane resolution to the msc.

Other systematic uncertainties were studied extensively in the previous publications on this subject [9, 10]. All were shown to be negligible compared to the uncertainty in determining the reaction plane. The shaded bands in the figures here represent the same uncertainty determined by a comparison of measurements with 1^{st} and 2^{nd} harmonic event planes.

For the simplified case of pure elliptic flow ($v_2 > 0$) + an added CME signal ($|a_1| > 0$), we have also verified through Monte Carlo simulations that the msc with respect to the sub-event planes corrected by the sub-event plane resolution is equivalent to the msc with respect to the reaction plane.

V. RESULTS

Larger charge separation fluctuations perpendicular to rather than parallel to the event plane can be seen by comparing distributions of $\Delta Q_{\rm OUT}$ to $\Delta Q_{\rm IN}$ as shown in Fig. 2 for the $40-50\%$ centrality bin. Figure 3 shows the difference over the mean of the RMS values ($\frac{\rm RMS_{OUT}-RMS_{IN}}{(\rm RMS_{OUT}+RMS_{IN})/2}$) versus centrality. The CME will cause wider out-of-plane distributions, however, $\mathcal{P}$-even processes may also cause the same feature (e.g. the decays of resonances with sizable v_2). Figures 2 and 3 are not corrected for the event plane resolution, however they clearly demonstrate larger charge separation fluctuations perpendicular rather than parallel to the event plane. Presumably, the difference between in-plane and out-of-plane distributions should be even larger if the ΔQ distributions are measured with the true reaction plane. In this paper, we would continue with other experimental observables to which the correction for the event plane resolution is easy to apply.

Figure 4 presents $\langle \sin(\phi_\alpha - \Psi_1)\rangle$ for positive and negative charges. Such a measure is sensitive to global parity violation of the strong interactions, i.e. a preference of charge separation orientation relative to the angular momentum orientation of the system. The results of Fig. 4 do not show a significant charge dependence. The mean values of both positive and negative charges are less than 5×10^{-4} at the 95% confidence level. For the most central and peripheral collisions we observe non-zero values for a_1. However, the values have the same sign for both charge types which is inconsistent with a global violation of parity.

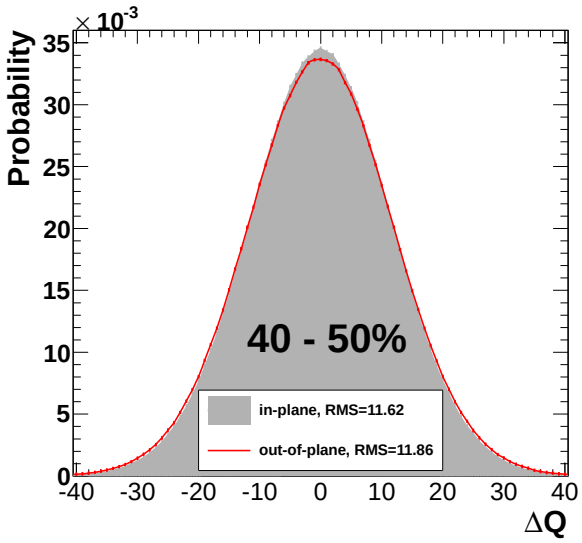

FIG. 2: (Color online) Sample ΔQ distributions for the 40-50% centrality Au+Au collisions at $\sqrt{s_{\rm NN}}$= 200 GeV. Not corrected for event plane resolution. The statistical uncertainties of the RMS values are negligible compared with the difference ΔRMS, as shown in detail in Fig. 3.

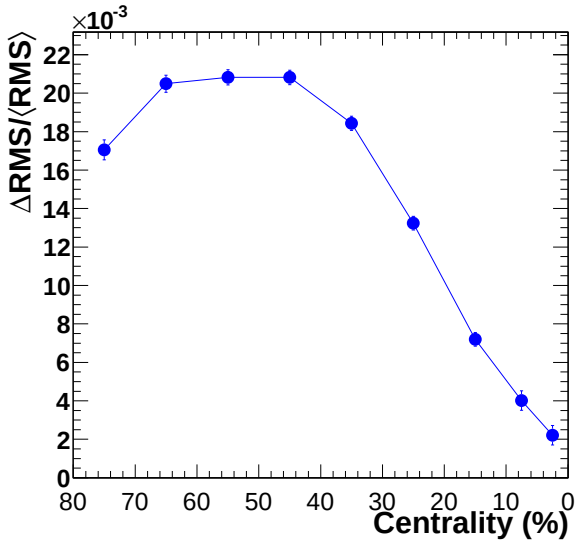

FIG. 3: (Color online) $\Delta{\rm RMS}^{\Delta Q}/\left\langle{\rm RMS}^{\Delta Q}\right\rangle$ versus centrality for Au+Au collisions at $\sqrt{s_{\rm NN}}$= 200 GeV. Not corrected for event plane resolution. Errors are statistical only.

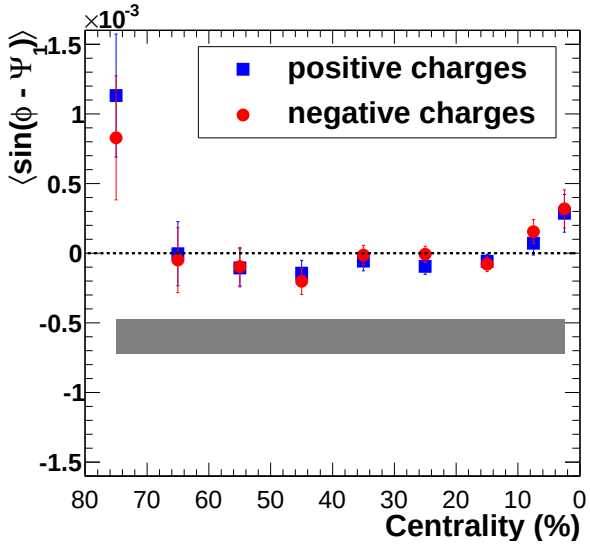

FIG. 4: (Color online) $\langle \sin(\phi_\alpha - \Psi_1) \rangle$ for positive and negative charges versus centrality for Au+Au collisions at $\sqrt{s_{\rm NN}}$= 200 GeV. Shaded area represents the systematic uncertainty for both charge types obtained by comparing correlations from positive and negative pseudorapidity.

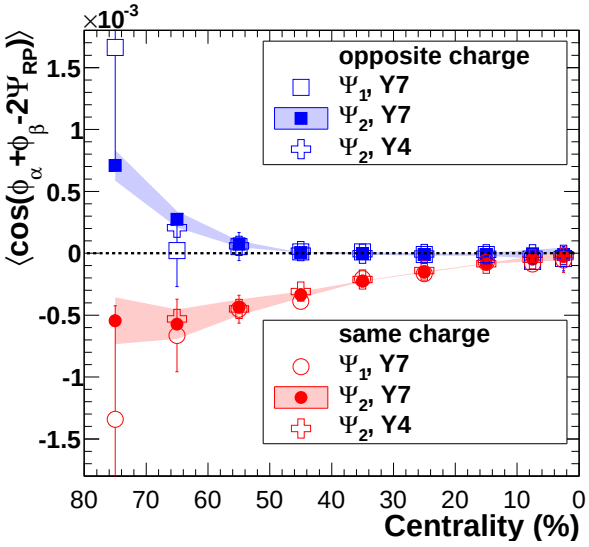

FIG. 5: (Color online) Three-point correlator, Eq. 1, measured with 1st and 2nd harmonic event planes versus centrality for Au+Au collisions at $\sqrt{s_{\rm NN}}$= 200 GeV. Shown with crosses are our previous results from the 2004 RHIC run (Y4) [9, 10]. The Y4 run used a second harmonic event plane. Y4 and Y7 Ψ_2 results are consistent within statistical errors. Shaded areas for the 2nd harmonic points represent the systematic uncertainty of the event plane determination. Systematic uncertainties for the 1st harmonic points are negligible compared to the statistical ones shown.

The three-point correlator measured with 1st and 2nd harmonic event planes is shown in Fig. 5. We find consistency between correlations obtained with both event plane types. As the pseudorapidity gap between the ZDC-SMD(Ψ_1) and the TPC(particles α and β) is rather large ($\sim$ 7 units in η) , we find "direct" three-particle effects (clusters) to be an unlikely source for the signal. This is an indication that the signal is likely a genuine correlation with respect to the reaction plane. Also shown for comparison in Fig. 5 are our previous results from the 2004 RHIC run [9, 10] which are consistent with the current results within statistical errors.

The modulated sign correlations are compared with the three-point correlator in Fig. 6. It is evident that the msc is able to reproduce the same trend as the three-point correlator although their magnitudes differ slightly. It is also clear that the correlation magnitude for same charge pairs is larger than for opposite charge pairs for both correlators. The charge combinations of ++ and −− are consistent with each other for the msc (not shown here), just like the case for the three-point correlator [10]. We also plot the model calculation of THERMINATOR [21] to be discussed later.

Before any possible interaction with the medium, the CME is expected to generate equal correlation magnitudes for same and opposite charge pairs. It was previously supposed that medium suppression of back-to-back phenomena could be responsible for this *magnitude asymmetry* [9, 10]. Oppositely charged pairs from the CME may not freeze out back-to-back, but instead with one of the particles deflected closer to the event plane due to multiple scattering within the medium. This is most likely to occur for the particle traversing the largest path length through the medium. However, when we weight all azimuthal regions of charge separation equally, as with the msc in Fig. 6, we do not recover a magnitude symmetry.

The two terms of the msc in Eq. 9 are shown in Fig. 7. We observe that same and opposite charge correlations in the ΔN term have very similar magnitudes, but opposite signs for all centrality bins. This feature is expected from the construction of the ΔN term due to the relatively large and approximately equal positive and negative charge multiplicities. A model calculation including statistical+dynamical fluctuations of particle azimuthal distributions should be performed in order to rule out $\mathcal{P}$-even explanations. The Δmsc term has a similar magnitude for same and opposite charge correlations, indicating a charge-independent background for the correlations. Thus, the source of the magnitude asymmetry between same and opposite charge correlations about zero as shown in Fig. 6 is isolated in the Δmsc term (Note that the sum of both terms yields the total msc). To further investigate the source of this background, we plot $-v_2/N$, a simplified estimate of the effect due to momentum conservation and elliptic flow [22]. Here v_2 was introduced in Eq. 2, and the values are from Ref. [23]. N represents the total number of produced particles, but in this practice we only counted those within $|\eta| < 1$. $-v_2/N$ well matches the Δmsc term for $0-50\%$ collisions. MEVSIM is a Monte Carlo event generator, developed for STAR simulations [24]. A model calculation of MEVSIM with

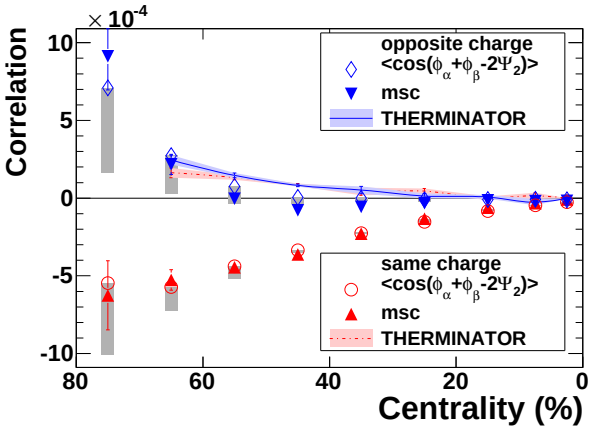

FIG. 6: (Color online) Modulated sign correlations (msc) compared to the three-point correlator versus centrality for Au+Au collisions at $\sqrt{s_{\rm NN}}$= 200 GeV. Shown with triangles is the msc, Eq. 5. The systematic uncertainties will be shown in detail in Fig. 7. Diamonds and circles show the three-point correlator, Eq. 1, and the grey bars reflect the conditions of $\Delta p_T > 0.15$ GeV/c and $\Delta\eta > 0.15$ applied to the three-point correlator, to be discussed in the text. For comparison, the model calculation of THERMINATOR [21] is also shown.

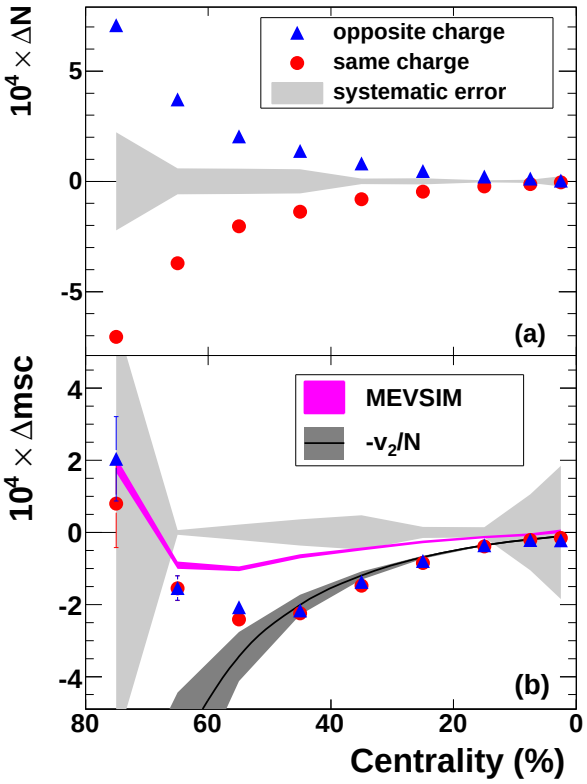

FIG. 7: (Color online) The msc split into 2 composite parts versus centrality for Au+Au collisions at $\sqrt{s_{\rm NN}}$= 200 GeV. Shaded areas represent the systematic uncertainty due to the event plane determination. For comparison with the Δmsc term, we also put $-v_2/N$ and the model calculation of MEVSIM [24], to be described in the text.

the implementation of v_2 and momentum conservation qualitatively describes the data trend.

We now present the composite parts of the three-point correlation, Eq. 1, differentially versus η and p_T. Figure 8 presents the three-point correlator versus the average η of particles α and β ($\langle\eta\rangle$) and absolute value of the difference ($|\Delta\eta|$). Figure 9 shows the same composite parts versus $\langle p_T\rangle$ and Δp_T. The subtraction of out-of-plane from in-plane composite parts yields the original three-point correlator while the sum yields a two particle correlation, $\langle\cos(\phi_\alpha - \phi_\beta)\rangle$. The split correlations reveal the underlying $\mathcal{P}$-even background affecting both composite parts as each part is sensitive to event plane independent correlations. We see that in each case the functional shape of in-plane and out-of-plane parts are similar. The magnitudes of in-plane and out-of-plane parts are more different for same charge pairs.

Femtoscopic correlations at low relative momentum which are related to quantum interference ("HBT") and final-state-interactions (Coulomb dominated) are visible in Figs. 8a-9b. The sharp increase of the correlation strengths for the lowest bins in Figs. 8b, 9a, and 9b are due to the combination of quantum interference in the same charge channel and the final-state-interactions in both channels. Low relative momentum in the transverse plane is clearly best visible in Fig. 9b for low values of $|\Delta p_T|$. The same phenomena are also visible for low values of $\langle p_T\rangle$ since these values best isolate low values of $|\Delta p_T|$. Low relative momentum along the beam axis is clearly visible in Fig. 8b for low values of $|\Delta\eta|$. The same phenomena are only visible for the larger values of $\langle\eta\rangle$ in Fig. 8a since η is signed. That is, the lowest values of $\langle\eta\rangle$ contain a substantial fraction of pairs with the opposite sign of η and therefore large relative momentum along the beam axis.

We also observe that the positive signal for opposite charge correlations observed in the peripheral bins of Fig. 6 ($\langle\cos(\Delta\phi_\alpha)\cos(\Delta\phi_\beta) - \sin(\Delta\phi_\alpha)\sin(\Delta\phi_\beta)\rangle$) is largely found in the kinematic regions of Figs. 8a-9b where femtoscopic correlations are prominent. In Fig. 6, femtoscopic correlations are qualitatively demonstrated by the model calculation of THERMINATOR [21]. THERMINATOR is a Monte Carlo event generator designed for studying of particle production in relativistic heavy-ion collisions, and includes estimates of the effects of resonance decays, quantum interference, final-state-interactions and collective motions. To suppress the contribution from femtoscopic correlations, we applied the conditions of $\Delta p_T > 0.15$ GeV/c and $\Delta\eta > 0.15$ to the three-point correlator, shown with the grey bars in Fig. 6. Femtoscopic correlations are sensitive to the size of the emission volume at freeze-out [25, 26]. The difference between in-plane and out-of-plane correlations in the kinematic region with prominent femtoscopic correlations can be due to a difference in the emission volumes probed by in and out-of-plane parts. Such a difference may arrise from an azimuthally anisotropic freeze-out distribution

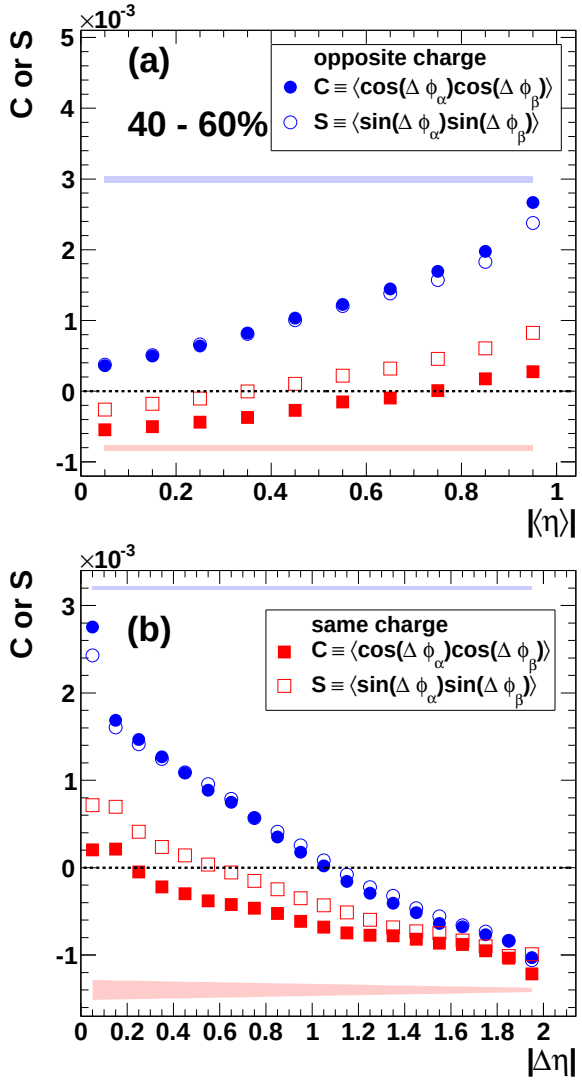

FIG. 8: (Color online) Three-point correlations split up into out-of-plane ($\langle\sin(\Delta\phi_\alpha)\sin(\Delta\phi_\beta)\rangle$) and in-plane ($\langle\cos(\Delta\phi_\alpha)\cos(\Delta\phi_\beta)\rangle$) composite parts for $40-60\%$ Au+Au collisions at $\sqrt{s_{\rm NN}}$= 200 GeV. (a) shows the correlations versus $\langle\eta\rangle = (\eta_\alpha+\eta_\beta)/2$. (b) shows the correlations versus $|\Delta\eta| = |\eta_\alpha-\eta_\beta|$. Statistical errors are smaller than the symbol size. Systematic errors are given by the shaded bands and apply only to the difference of in-plane and out-of-plane parts.

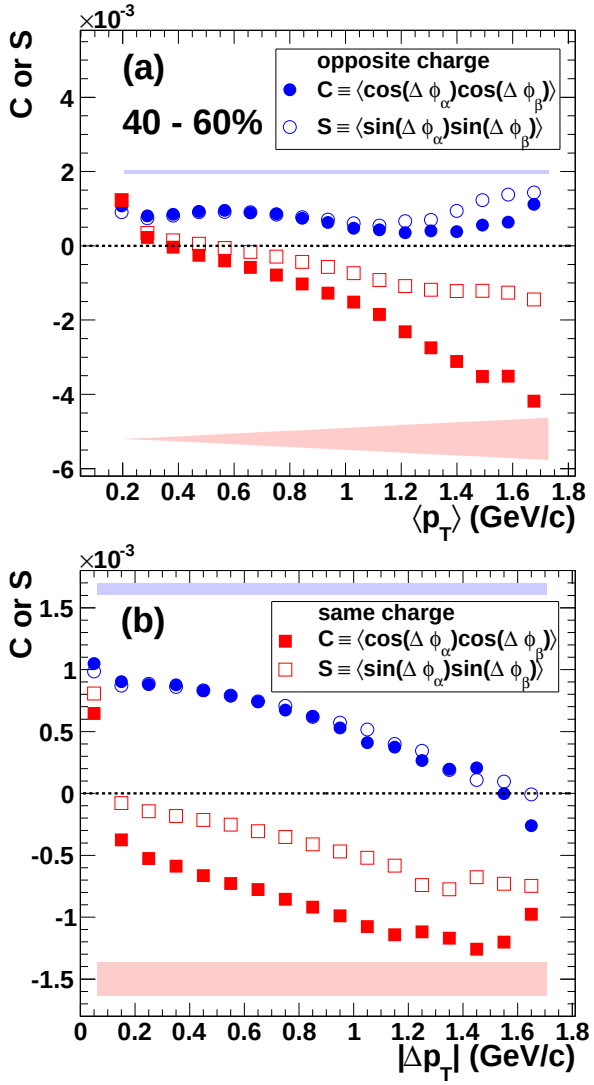

FIG. 9: (Color online) Three-point correlations split up into out-of-plane and in-plane composite parts for $40-60\%$ Au+Au collisions at $\sqrt{s_{\rm NN}}$= 200 GeV. (a) shows the correlations versus $\langle p_T\rangle = (p_{T,\alpha}+p_{T,\beta})/2$. (b) shows the correlations versus $|\Delta p_T| = |p_{T,\alpha}-p_{T,\beta}|$. Statistical errors are smaller than the symbol size. Systematic errors are given by the shaded bands and apply only to the difference of in-plane and out-of-plane parts.

coupled with elliptic flow.

VI. SUMMARY

Correlations sensitive to charge separation in heavy-ion collisions have been presented. Consistency between correlations with respect to 1^{st} and 2^{nd} harmonic event planes demonstrates that the signal is likely to be related to the reaction plane. Also presented was a reduced version of the three-point correlation in which all regions of charge separation are weighted equally. The same qualitative signal was found to persist in this scheme as well. The signal shown in Fig. 6 is largely determined by the sign ($\pm$) of the cosine and sine functions in Eq. 1.

We also explicitly counted units of charge separation with which we could better understand the source of the opposite charge suppression. A parity conserving background, due to momentum conservation and collective flow, is more likely to explain the suppression rather than the medium induced back-to-back suppression previously supposed [9, 10]. A comparison of the RMS values for $\Delta Q_{\rm OUT}$ and $\Delta Q_{\rm IN}$ suggests greater charge separation fluctuations perpendicular to rather than parallel to the event plane. The CME as well as $\mathcal{P}$-even processes such

as the decays of resonances with sizable v_2 may both contribute to this feature.

The differential analysis of the in-plane and out-of-plane parts of the three-point correlator versus η and p_T reveals femtoscopic contributions at low relative momentum. The positive signal in Fig. 6 for opposite charge correlations in peripheral collisions is largely found in the low relative momentum regions of Fig. 8 and Fig. 9. This can possibly be explained by the final-state-interactions ($\mathcal{P}$-even) of different emission volumes probed by in-plane and out-of-plane parts.

Excluding low relative momentum pairs significantly reduces the positive contributions to opposite charge correlations in Fig. 6. However, the difference between same and opposite charge correlations remains largely unchanged and consistent with the expectations of the CME. $\mathcal{P}$-even local charge conservation coupled to elliptic flow modeled by charge balance functions has also been shown to generate same charge three-point correlations comparable to the observed one [19]. A careful calculation of the mentioned $\mathcal{P}$-even backgrounds needs to be made before a further assessment of the Chiral Magnetic Effect can be made in heavy-ion collisions.

Acknowledgments

We thank the RHIC Operations Group and RCF at BNL, the NERSC Center at LBNL and the Open Science Grid consortium for providing resources and support. This work was supported in part by the Offices of NP and HEP within the U.S. DOE Office of Science, the U.S. NSF, the Sloan Foundation, CNRS/IN2P3, FAPESP CNPq of Brazil, Ministry of Ed. and Sci. of the Russian Federation, NNSFC, CAS, MoST, and MoE of China, GA and MSMT of the Czech Republic, FOM and NWO of the Netherlands, DAE, DST, and CSIR of India, Polish Ministry of Sci. and Higher Ed., National Research Foundation (NRF-2012004024), Ministry of Sci., Ed. and Sports of the Rep. of Croatia, and RosAtom of Russia.

[1] T. D. Lee and C. N. Yang, Phys. Rev. **104**, 254 (1956).
[2] C. Vafa and E. Whitten, Phys. Rev. Lett. **53**, 535 (1984).
[3] T. D. Lee, Phys. Rev. D **8**, 1226 (1973).
[4] T. D. Lee and G. C. Wick, Phys. Rev. D **9**, 2291 (1974).
[5] D. Kharzeev, Phys. Lett. B **633**, 260 (2006).
[6] D. Kharzeev and A. Zhitnitsky, Nucl. Phys. A **797**, 67 (2007).
[7] D. Kharzeev, L. D. McLerran and H. J. Warringa, Nucl. Phys. A **803**, 227 (2008).
[8] K. Fukushima, D. Kharzeev and H. J. Warringa, Phys. Rev. D **78**, 074033 (2008).
[9] B. I. Abelev *et al.* (STAR Collaboration), Phys. Rev. Lett. **103**, 251601 (2009).
[10] B. I. Abelev *et al.* (STAR Collaboration), Phys. Rev. C **81**, 054908 (2010).
[11] B. I. Abelev *et al.* (ALICE Collaboration), Phys. Rev. Lett. **110**, 012301 (2013).
[12] K. H. Ackermann *et al.* (STAR Collaboration), Nuclear Instruments and Methods in Physics Research A **499**, 624 (2003).
[13] J. Adams *et al.* (STAR Collaboration), Phys. Rev. C **73**, 034903 (2006).
[14] L. Adamczyk *et al.* (STAR Collaboration), Phys. Rev. Lett. **108**, 202301 (2012).
[15] S. Voloshin, Phys. Rev. C **70**, 057901 (2004).
[16] A. M. Poskanzer and S. Voloshin, Phys. Rev. C **58**, 1671 (1998).
[17] J. -Y. Ollitrault, A. M. Poskanzer and S. A. Voloshin, Phys. Rev. C **80**, 014904 (2009).
[18] S. Pratt, S. Schlichting and S. Gavin, arXiv:1011.6053.
[19] S. Schlichting and S. Pratt, Phys. Rev. C **83**, 014913 (2011).
[20] I. Selyuzhenkov and S. Voloshin, Phys. Rev. C **77**, 034904 (2008).
[21] A. Kisiel *et al.*, Comput. Phys. Commun. **174**, 669 (2006). The starting time of hydrodynamics was 0.25 fm/c, and the freeze-out temperature, 145 MeV. The initial central temperature varied between 500 and 279 MeV from central to peripheral collisions.
[22] A. Bzdak *et al.*, Phys. Rev. C **83**, 014905 (2011).
[23] J. Adams *et al.* (STAR Collaboration), Phys. Rev. C **72**, 14904 (2005).
[24] R. L. Ray and R. S. Longacre, arXiv:nucl-ex/0008009 and private communication.
[25] G. I. Kopylov and M. I. Podgoretsky, Sov. J. Nucl. Phys. **15**, 219 (1972); G. I. Kopylov, Phys. Lett. B. **50**, 472 (1974); M. I. Podgoretsky, Sov. J. Part. Nucl. **20**, 266 (1989).
[26] G. Goldhaber, S. Goldhaber, W. Lee, A. Pais, Phys. Rev. **120**, 325 (1960).